Study of Effective Particle Charging Regions in a Corona Discharge in an Electrostatic Precipitator

Yoshihiro Kawada[1], Akinori Zukeran[2]

[1]Polytechnic University of Japan, Japan; [2]Kanagawa Institute of Technology;
kawada@uitec.ac.jp
Keywords: Corona discharge, Particle charge, Electric-field distribution

Abstract

Every electrostatic precipitator uses a corona discharge to charge the material particles to be precipitated, and two particle charging processes occur in it: field charging and diffusion charging. The aim of this study is to evaluate the dependence of particle charging on the number density of negative ions and the electric field distribution. For this work, we replaced the space-charge with the number density of negative ions. We used a wire–plate-type electrode structure for the calculation model, applying negative DC high voltage to the wire electrode, and grounding the plate electrode. We previously calculated the distributions of the electric field and of the number density of negative ions using a two-dimensional finite-element method. In the present work, we calculate both the field charging and diffusion charging processes based on those results. However, we did not include the negative ions lost during particle charging in these calculations. Our results show that electric field charging tends to occur directly under the wire electrode, while diffusion charging is more widespread. For a constant-power discharge, we found that, although increasing only the voltage increases the electric field that accelerates the charges, it decreases the space-charge density. We also found that larger particles tend to be charged closer to the grounded plate electrode than in the vicinity of the wire electrode.

1. Introduction

A corona discharge is important for charging particles in an electrostatic precipitator. Such discharges have been used both in one-stage electrostatic precipitators

that are appropriate for high particle concentrations and low gas flow velocities and in two-stage electrostatic precipitators that are appropriate for low particle concentrations and high gas flow velocities. Although every electrostatic precipitator uses a corona discharge for particle charging, the role of the corona discharge in a one-stage electrostatic precipitators includes both charging and collecting particles, while in a two-stage electrostatic precipitator it is only employed as a precharger for charging particles. Both an electric field and space-charge are necessary for particle charging, and the distributions of the electric field and the space-charge density depend upon the electrode shape, the gas flow, and the applied voltage.

Particle charging in an electrostatic precipitator involves two processes: field charging and diffusion charging [1, 2]. Many papers have considered these two processes theoretically. In general, diffusion charging dominates for particles with diameters of 2 μm or less, while field charging dominates for particles larger than 2 μm [2, 3]. Numerous studies of the space-charge and electric field distributions in corona discharge have been carried out to determine the particle-collection efficiencies of precipitators [3, 4, 5]. There has also been research on an electrostatic precipitator in which the simple corona discharge of a precharger has been replaced with a more effective shape or an electron beam [6, 7, 8]. The charge simulation method for electric field [9], study from the voltage-current characteristics utilizing any experimental formulas [10], and study for the formation of ionic wind [11] are recent methods used in studies on the charge transfer in the corona discharge. Moreover, there is a study with the finite element method for corona discharge [12]. However, few investigations have focused on the particle charging process itself—including both diffusion charging and field charging—to determine its effect on the particle-collection efficiency.

The aim of this study is to determine the regions effective for particle charging from the distributions of the number density of negative ions and the electric field. For this purpose, we replaced the space-charge with the number density of negative ions. We used a wire–plate-type electrode structure as the calculational model, applying negative DC high voltage to the wire electrode and grounding the plate electrode. The position of this experimental device is the precharger of the home-use air-cleaner, or laboratory-scale one-stage type electrostatic precipitator for feasibility investigation. We had previously calculated the distributions of the electric field and of the number density of negative ions using a two-dimensional finite-element method [13]. For the present study, we extracted data from these computations at 1 mm intervals in the aim of calculation with the constant residence time. However, the distribution of the number density of negative ions we used in this work does not include those lost during particle charging. For the same discharge power, we calculated particle charging separately for cases in which only the applied voltage was increased, or only the discharge current was increased. We also determined which regions of the discharge area between the high voltage electrode and the grounded electrode are most effective for particle charging, as we expect the charging efficiency to be improved by distributing gas flow primarily to these regions. These results lead to possibilities for improving the electrode shape and structure and the applied voltage in an electrostatic precipitator.

2. Assumed model and previous research

The experimental model apparatus is shown in Fig. 1, and we have based the calculational model on it. This one-stage precharger consists of a high voltage wire electrode and grounded plate electrodes. The grounded electrodes are 80 mm long, which is long enough to eliminate edge effects. The discharge current at the same applied voltage is the highest, when the grounded electrode length is three times the distance between of the wire to plate electrode. Because, effects of the electrode area and electrode edges are superimposed [13]. The grounded electrode of 80 mm is 5.3 times the distance between the wire and plate electrode. It is believed that the discharge is not significantly affected of edges by the effects of the grounded electrode margins. We applied voltage a negative DC high voltage to the wire electrode. The experimental discharge condition was −10.2 kV and 0.28 mA DC. This discharge current was measured in the room atmosphere. These results are the same as those from our previous paper [13], although we recalculated the initial charge density Ni to be 3.94×10^{14} m^{-3} for a discharge current 0.28 mA. In calculating the density of negative ions, negative values have often arisen due to partial divergences; we replaced such unphysical negative values of the ion number density by zero in subsequent calculations.

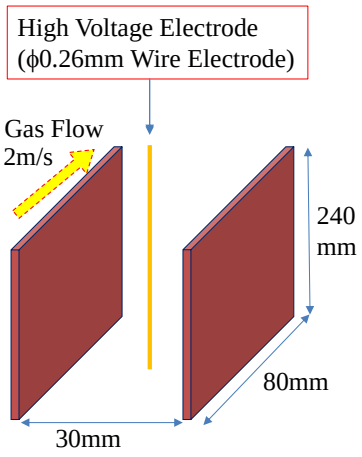

Fig. 1. Schematic illustration of a precharger.

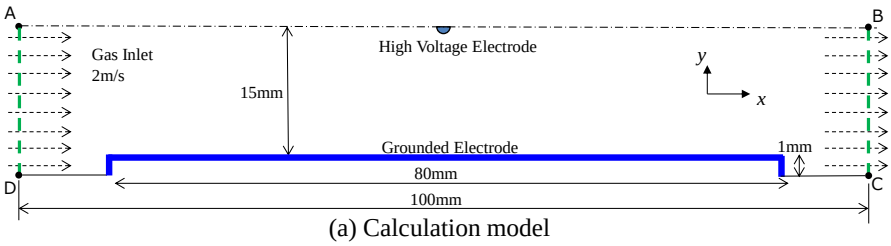

(a) Calculation model

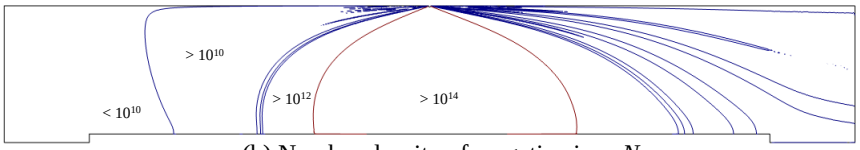

(b) Number density of negative ions *Nn*

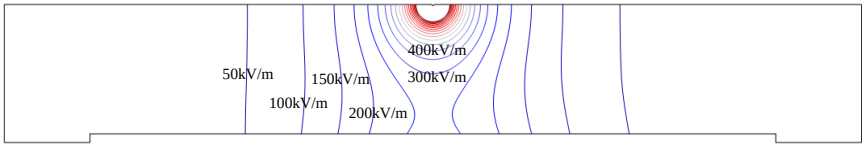

(c) Electric field distribution *E*

Fig. 2. (a) Calculational model and the resulting (b) number density of negative ions and (c) electric-field distribution [9]. The numbers in panel (b) are in units of particles m^{-3}.

3. Calculational model

We sampled data from Figs. 2 (b) and (c) to obtain the number density of negative ions and the electric field distribution, respectively, at 1 mm intervals, and we inserted these values into the equations below.

As noted above, particle charging involves two processes: field charging, as ions collide with a material particle under the influence of the Coulomb force, and diffusion charging, as ions collide with the particle due to thermal diffusion. The total particle charge q is the sum of the diffusion charge q_{dif} and the field charge q_f:

$$q = q_{dif} + q_f \ . \qquad (1)$$

The diffusion charge q_{dif} is given by equation (2) below, where q^* is the charge constant given by equation (3), and τ_c' is the charging time constant given by equation (4). We substituted the value $\tau_c' = 10^{99}$ s when there is no charging.

$$q_{dif} = q^* ln\left(1 + {}^{t}/_{\tau_c'}\right) \qquad (2)$$

$$q^* = \frac{4\pi\varepsilon_0 akT}{e} \qquad (3)$$

$$\tau_c' = \frac{4\varepsilon_0 kT}{aC_i n_i e^2} \qquad (4)$$

In these equations, $k = 1.38\times10^{-23}$ J·K^{-1} is the Boltzmann constant, $\varepsilon_0 = 8.85 \times 10^{12}$ F/m is the permittivity of free space, T is the absolute temperature, a is the radius of the target particle, and $e = 1.6 \times 10^{-19}$ C is the elementary unit of charge. For the number density n_i of ions we used the ion number density N_n. The quantity C_i in

equation (4) is the root-mean-square ion thermal velocity in m/s, which we calculated from equation (5) below,

$$C_i = \sqrt{3kT/m_i}, \quad (5)$$

where m_i is the ion mass in kg. Using a composition of 78% nitrogen (molecular weight 28), 21% oxygen (molecular weight 32), and 1% argon (atomic weight 40), we obtained 28.96 g divided by Avogadro's number as the mass of 1 mol of air molecules. We used the value C_i = 502.87 m/s for the thermal velocity in our subsequent calculations.

The field charge q_f is given by equation (6) below in terms of the saturated charge amount q_∞ in coulombs (C), given by equation (7), and the chargeability is determined by the charging time constant τ_i in seconds (s), given equation (8). We assigned the charging time constant the value 10^{99} s when there is no charging.

$$q_f = q_\infty \frac{t/\tau_i}{1+t/\tau_i} \quad (6)$$

$$q_\infty = 4\pi\varepsilon_0 \frac{3\varepsilon_s}{\varepsilon_s+2} a^2 E \quad (7)$$

$$\tau_i = \frac{4\varepsilon_0}{\mu\rho_i} \quad (8)$$

In these equations, E is the charging electric field in V/m, t = 0.5 msec is the residence time determined by the assumed gas flow velocity of 2 m/s and the data-sampling interval of 1 mm, and we assumed the relative permittivity to be ε_s = 5.5, which is appropriate for carbon powder. The quantity ρ_i is the product of the elementary charge and the ion density N_n, and $\mu = 1.43 \times 10^{-4}$ m^2/V·s is the mobility of the negative ions.

For each type of charging and electric field distribution, we obtained the contour diagrams shown using MATLAB Simulink.

4. Results and Discussion

4.1. Diffusion charging and field charging

We obtained the contour diagrams shown in Fig. 3 from the data sampled from Fig. 2. The distribution of the ion number density is spindle-shaped, while the electric field distribution is spread in the vertical direction.

The characteristics of the experimental discharge current and of the calculations reported below are shown in Fig. 4. In this section, we first discuss calculations using an applied voltage of 10.2 kV and a discharge current of 0.28 mA. We then calculated and compared the results when the power is multiplied by 1.4, increasing the voltage and current to 10.75 kV and 0.32 mA, respectively. In addition, in the following section, we calculated the charging characteristics at 10.2 kV and 0.39 mA, which is 1.4 times the current only, and at 14.3 kV and 0.28 mA, which is 1.4 times the voltage only. The initial charge density Ni is 5.49×10^{14} m^{-3} for a discharge current 0.39mA and applied voltage 10.2 kV, and 2.83×10^{14} m^{-3} for a discharge current 0.28mA and applied voltage 14.3 kV.

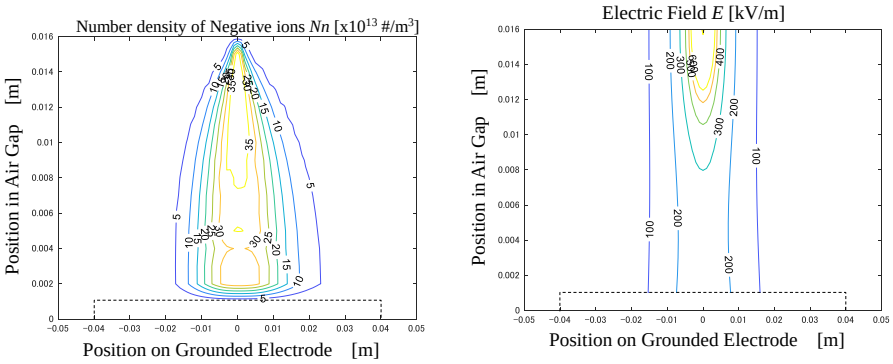

(a) Number density of Negative ions (b) Electric Field

Fig. 3. Calculation of (a) the number density of negative ions and (b) the electric field for the treated model. (Using the same data as shown in Fig. 2.)

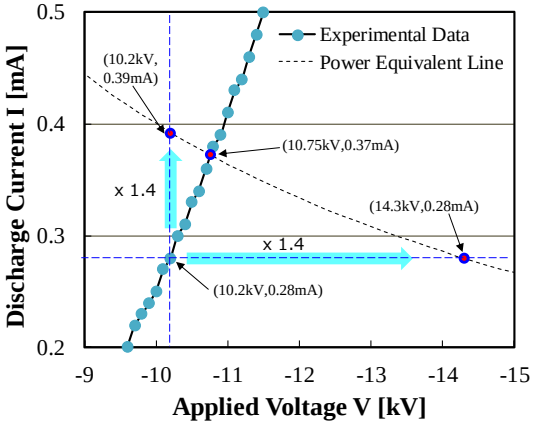

Fig. 4. Discharge current as a function of applied voltage.

For an applied voltage of 10.2 kV and a discharge current of 0.28 mA, the charging distributions for particle sizes of 0.05 μm and 5 μm are shown in Fig.5 and 6 respectively. These figures show the amount of particle charging that occurs when the particles remain in the corona discharge for 5 ms. They have monodisperse particle distributions.

Equation (4) shows that the time constant for diffusion charging is inversely proportional to the charge density. When this time constant is small, particles can thus be charged very rapidly. In addition, diffusion charging does not depend on the electric field strength, as shown by equations (2) and (3). Therefore, the region in which diffusion charging occurs is similar to the region in which the space-charge distribution exists. On the other hand, electric field charging has a narrow spatial distribution that reflects the electric field distribution because the saturated charge constant depends on the electric field strength, as shown by equation (7). However, since the field charging time constant is inversely proportional to the charge density, it is also affected by the charge density.

Equation (3) shows that the diffusion charge constant q^* is proportional to the particle size, while equation (7) shows that the field charge constant q_∞ is proportional to the square of the particle size. When we increased the particle size from 0.05 μm to 5 μm, the particle charge distributions shown in Fig. 5 (b) and Fig. 6 (b) therefore differed by four orders of magnitude, even though the shapes of the distributions were similar. Compared with field charging, diffusion charging was about five times higher near the wire electrode at a particle size of 0.05 μm, but it was about 40% lower at a particle size of 5 μm. This difference shows that diffusion charging is more effective for fine particles, while field charging is more important for larger particles.

We also found that the region close to the wire dominates in field charging, while a relatively wide region dominates in diffusion charging due to spreading of the space-charge. Thus, the regions in which particle charging occurs differ for field charging and diffusion charging.

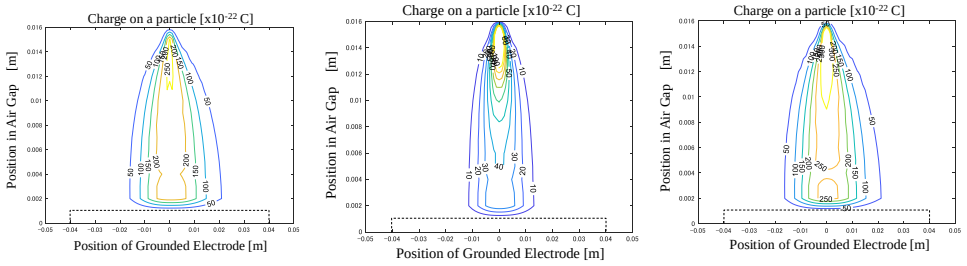

(a) Diffusion Charging (b) Field Charging (c) Total Charging

Fig.5 Calculated particle charging with diffusion charging and field charging. (Particle size 0.05 μm)

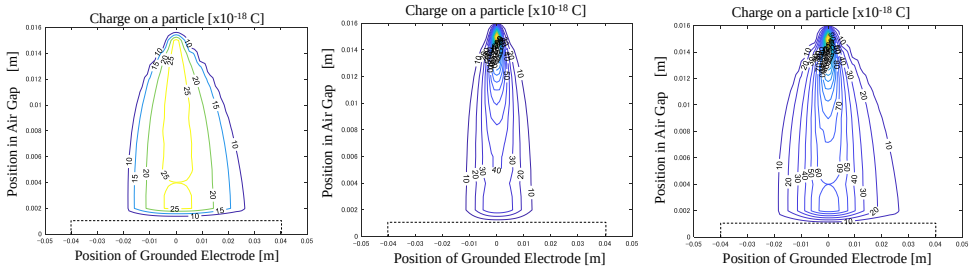

(a) Diffusion Charging (b) Field Charging (c) Total Charging

Fig.6 Calculated particle charging with diffusion charging and field charging. (Particle size 5 μm)

4.2. Increased discharge power with constant voltage or constant current

In this section, we discuss the charging characteristics for the same discharge power but different voltage or current. When the applied voltage is multiplied by 1.4 while the discharge current remains the same as in Figs. 5 and 6, the charging characteristics are shown in Figs. 7 and 8. Diffusion charging has decreased in this case because the increase in the applied voltage has increased the charge mobility. Field charging increased slightly, but the total amount of charging hardly changed. This occurs because the high voltage wire electrode is small in diameter and does not lead to an increase in the electric field strength throughout the entire space when

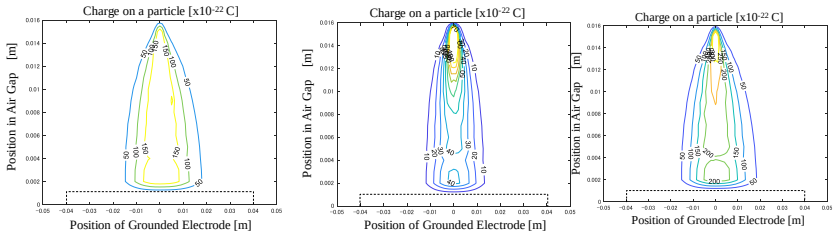

(c) Diffusion Charging (b) Field Charging (c) Total Charg-

Fig.7. (14.3kV,0.28mA) Calculated particle charging with diffusion charging and field charging. (Particle size 0.05 μm)

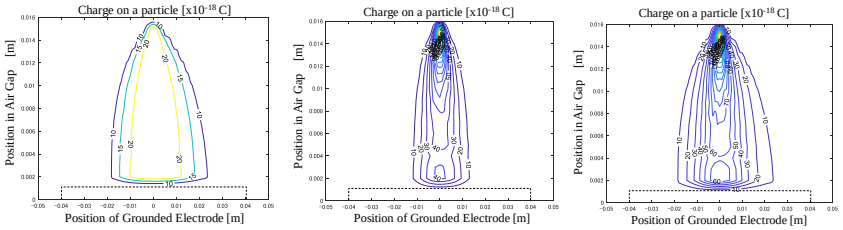

(a) Diffusion Charging (b) Field Charging (c) Total Charging

Fig.8. (14.3kV,0.28mA) Calculated particle charging with diffusion charging and field charging. (Particle size 5 μm)

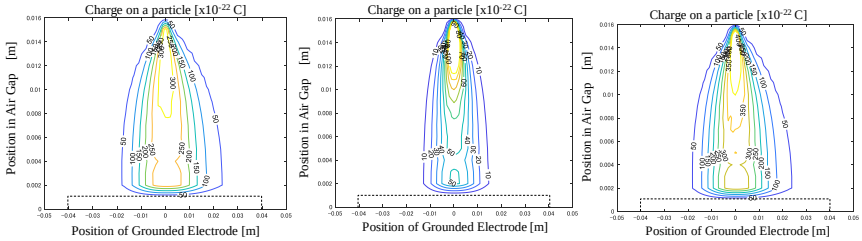

(a) Diffusion Charging (b) Field Charging (c) Total Charg-

Fig.9. (10.2kV,0.39mA) Calculated particle charging with diffusion charging and field charging. (Particle size 0.05 μm)

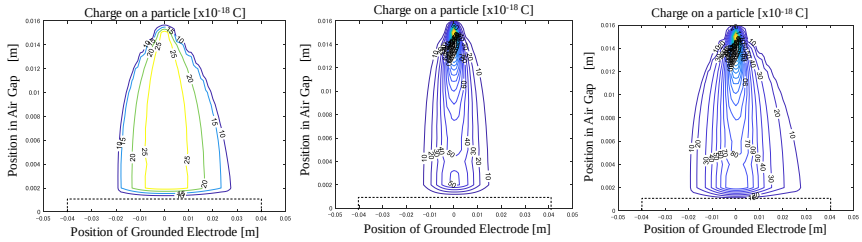

(a) Diffusion Charging (b) Field Charging (c) Total Charging

Fig.10. (10.2kV,0.39mA) Calculated particle charging with diffusion charging and field charging. (Particle size 5 μm)

the voltage is increased. Also, the electric field strength within the corona discharge is scarcely higher than that obtained when the corona-onset voltage is applied.

On the other hand, when the discharge current is multiplied by 1.4 with respect to Figs. 5 and 6, the charge characteristics are shown in Fig.9 and 10. In this case, diffusion charging of the fine particles has increased by about a factor of 1.4, and the effective charging region extends for some distance downstream. We also observed an increase of about 20% in field charging and an expansion of the field charging region. Consequently, the total amount of charging also increased.

Hence, we found that giving priority to an increase in the discharge current rather than in the voltage leads to an increase in particle charging. In particular, it is desirable that the precharger in a two-stage electrostatic precipitator be designed for a low applied voltage and a high discharge current.

4.3. Effective charge region

The particle charging regions we considered are shown in Fig.11. The calculation conditions are the same as for Fig. 5 (c). The particle charges obtained at various heights above the grounded electrode surface are shown in Fig.12 as a function of particle size. Fig.12 (a) shows the particle charges obtained directly under the wire electrode (the left dot-dashed red vertical line in Fig. 11), and Fig 12 (b) shows the results 20 mm downstream from Fig.12 (a) (the right dot-dashed red vertical line in Fig. 11). The particle charges decrease naturally as one proceeds downstream, although they remain approximately constant at heights of 3 to 9 mm above the grounded electrode. At a height of 6 mm above the grounded electrode, the electric field is 270 kV/m directly under the wire and 62 kV/m at a location 20 mm downstream. As one moves from a position directly under the wire to 20 mm downstream, the amount of particle charging decreases by about 1 digit at a height of 6 mm but by about 4 digits at a height of 15 mm. In other words, we found that the contribution of the electric field is low if the charge is present. When considering a precharger for a two-stage electrostatic precipitator, the ion distribution should thus be designed to be wide and the gas flow should be concentrated close to the grounded plate electrode at a high flow velocity.

We have also calculated the characteristics when an excess current is applied or when an excess voltage is applied. For example, we examined theoretically how the diameter of the wire electrode affects particle charging. Specifically, if a thicker wire electrode is used, we found that the applied voltage is increased, but the discharge current can be suppressed. On the other hand, the use of a thinner wire, spike, or sharp edge as the discharge electrode promotes the discharge. These calculation results can thus be used to deduce guidelines for the design of the discharge electrode.

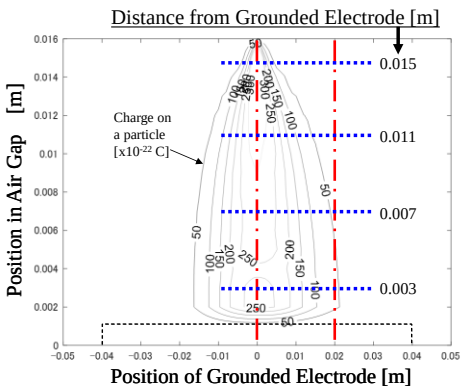

Fig.11 Analytical cut line of calculation model

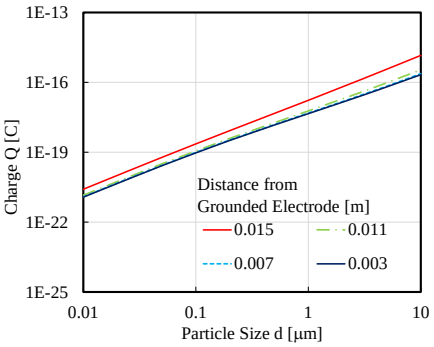

(a) 0mm (under the wire electrode)

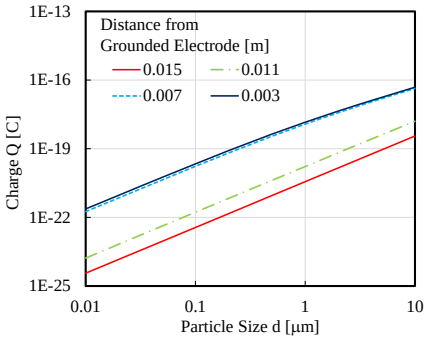

(b) 20mm

Fig.12 Particle charge as a function of particle size for various electrode position.

5. Concluding remarks

Based on the calculated distributions of the ion number density and the electric field of a corona discharge, we have studied the regions that are effective for particle charging in an electrostatic precipitator, including both electric field charging and diffusion charging. We found the following results:

(1) Since it depends on the distribution of the electric field, electric field charging tends to occur directly under the wire electrode, in contrast to diffusion charging. That is, large-sized particles are effectively charged just below the wire electrode.

(2) For the same discharge power, we considered separately a case in which only the current was increased and a case in which only the voltage was increased. We found that when only the voltage was increased, the electric field that accelerates the charges also increased, but the charge density is decreased. Therefore, we found that increasing only the electric field does not lead to an increase in the amount of particle charging.

(3) We also found that particles closer to the grounded plate electrode can be charged for longer periods of time than can those in the vicinity of the wire electrode. This occurs because the space-charge distribution spreads toward the grounded electrode.

We thus conclude that by matching the charge distribution and gas flow, the discharge electrode can be shaped to achieve more effective particle charging.

References

1. K.R.Parker edt. “Applied electrostatic precipitation,” Blackie Academic & Professional, pp.52-87, 1997.
2. B.Y.H.Liu, A.Kapadia “Combined field and diffusion charging of aerosol particles in the continuum regime” Journal of Aerosol Science, Vol. 9, pp.227-242, 1978.
3. J.S.Chang, A.J.Kelly, M.Joseph Crowley edt. “Handbook of electrostatic processes” Marcel Dekker, Inc., p. 445, 1995.
4. S. Oglesby, Jr., B. Grady Nichols “Electrostatic precipitation” Marcel Dekker, Inc., 1978.
5. J.Harry White “Industrial electrostatic precipitation” Addison-Wesley Publishing Company, Inc., p.128, 1963.
6. S.Masuda “Industrial applications of electrostatics” Journal of Electrostatics, Vol. 10, pp. 1-15, 1981.
7. J.S.Chang, C.A.McLinden, A.A.Berezin, P.C.Looy, T. Tanaka “Modelling of quadrupole cold precharger dust particle charging characteristics” Research reports of the Faculty of Engineering, Tokyo Denki University, No. 44, pp. 1-15, DEC.1996.
8. A.Mizuno, J.S.Clements, R.H.Davis “Use of an electron beam for particle charging” IEEE Transactions on Industry Applications, Vo. 26, No. 1, pp. 29-35, 1990.
9. M.Abdel-Salam, A.Hashem, E.Sidique “Characteristics of Negative Corona Discharge in Single-Needle- and Multi- Needle-to-Plane Configurations” International Journal of Plasma Environmental Science & Technology, Vol.7, No.2, pp.121-135, 2013
10. Antonio J.Conesa, Mario Sanchez “The Current–Voltage Characteristics of Corona Discharge in Wire to Cylinder in Parallel Electrode Arrangement” IEEE Transactions on Plasma Science, Vol.46, No.8, pp.3022-3030, 2018
11. Eric Moreau, Sonia Souakri, Romain Bellanger, Nicolas Benard “Ionic wind produced by a millimeter-gap DC corona discharge ignited between a plate and an inclined needle” International Journal of Plasma Environmental Science & Technology, Vol.15, e01001 (15pp). 2021
12. H.Ziedan, J.Tlusty, A.Mizuno, A.Sayed, A.Ahmed, R.Prochazka “Finite Element Solution of Corona I-V Characteristics in ESP with Multi Discharge Wires” International Journal of Plasma Environmental Science & Technology, Vol.5, No.1, pp.206-217, 2011
13. Y.Kawada, H.Shimizu, A.Zukeran “Numerical study of the suitable pre-charger grounded electrode length in two-stage-type electrostatic precipitators” IEEE Transactions on Industry Applications, Vol. 55, pp. 833-839, 2019.